Design of experiments

A statistical tool for PIV uncertainty quantification

Adatrao, S.; van der Velden, S.; van der Meulen, Mark-Jan; Cruellas Bordes, Marc; Sciacchitano, A.

DOI
10.1088/1361-6501/ac9541

Publication date
2023

Document Version
Final published version

Published in
Measurement Science and Technology

Citation (APA)
Adatrao, S., van der Velden, S., van der Meulen, M.-J., Cruellas Bordes, M., & Sciacchitano, A. (2023). Design of experiments: A statistical tool for PIV uncertainty quantification. *Measurement Science and Technology*, *34*(1), Article 015201. https://doi.org/10.1088/1361-6501/ac9541

Design of experiments: a statistical tool for PIV uncertainty quantification

OPEN ACCESS
IOP Publishing
Measurement Science and Technology
Meas. Sci. Technol. **34** (2023) 015201 (15pp)
https://doi.org/10.1088/1361-6501/ac9541

Design of experiments: a statistical tool for PIV uncertainty quantification

Sagar Adatrao[1,*], Simone van der Velden[1], Mark-Jan van der Meulen[2], Marc Cruellas Bordes[3] and Andrea Sciacchitano[1]

[1] Faculty of Aerospace Engineering, Delft University of Technology, Delft, The Netherlands
[2] Royal Netherlands Aerospace Center (NLR), Marknesse, The Netherlands
[3] German-Dutch Wind Tunnels (DNW), Marknesse, The Netherlands

E-mail: s.adatrao@tudelft.nl

Received 31 March 2022, revised 22 August 2022
Accepted for publication 27 September 2022
Published 20 October 2022

Abstract

A statistical tool called design of experiments (DOEs) is introduced for uncertainty quantification in particle image velocimetry (PIV). DOE allows to quantify the total uncertainty as well as the systematic uncertainties arising from various experimental factors. The approach is based on measuring a quantity (e.g. time-averaged velocity or Reynolds stresses) several times by varying the levels of the experimental factors which are known to affect the value of the measured quantity. Then, using Analysis of Variances, the total variance in the measured quantity is computed and hence the total uncertainty. Moreover, the analysis provides the individual variances for each of the experimental factors, leading to the estimation of the systematic uncertainties from each factor and their contributions to the total uncertainty. The methodology is assessed for planar PIV measurements of the flow over a NACA0012 airfoil at 15 degrees angle of attack considering five experimental factors, namely camera aperture, inter-frame time separation, interrogation window size, laser sheet thickness and seeding density. Additionally, the methodology is applied to the investigation by stereoscopic PIV of the flow at the outlet of a ducted Boundary Layer Ingesting propulsor. The total uncertainty in the time-averaged velocity as well as the constituent systematic uncertainties due to the experimental factors, namely camera aperture, inter-frame time separation, interrogation window size and stereoscopic camera angle, are quantified.

Keywords: PIV, uncertainty quantification, design of experiments (DOE), systematic uncertainties, ANOVA, factor analysis, wind tunnel measurements

(Some figures may appear in colour only in the online journal)

1. Introduction

Despite the quantification of the particle image velocimetry (PIV) uncertainty being the key to discern measurement errors from the true flow physics, PIV uncertainty quantification (UQ) is often hindered by the complexity of the measurement chain, which introduces errors from various sources such as particles, illumination, imaging and processing. Several *a-posteriori* approaches have been proposed for PIV UQ, such as particle disparity or image matching method (Sciacchitano *et al* 2013), correlation statistics approach (Wieneke 2015), moment of correlation plane strategy (Bhattacharya *et al* 2018), which evaluate the uncertainty directly from the computed displacement or velocity field. However, such approaches mostly focused on quantifying the uncertainty from random errors and were limited in

* Author to whom any correspondence should be addressed.

the quantification of the systematic uncertainty (Sciacchitano *et al* 2015, Neal *et al* 2015). Other approaches like uncertainty surface method (Timmins *et al* 2012) and cross-correlation peak ratio criterion (Charonko and Vlachos 2013) took systematic error sources into consideration. However, both the approaches rely on synthetic data to generate uncertainty surface or empirical model to calculate uncertainty which can lead to inaccurate uncertainty estimation for experimental data. Moreover, the main results of the 4th international PIV challenge (Kähler *et al* 2016) showed that, even for the same set of image recordings, large differences in the PIV results occurred among the participants due to the selection of the different processing parameters. Additionally, the systematic errors in PIV arise not only in the selection of the processing algorithm and the related parameters, but also during the data acquisition phase (Sciacchitano 2019). For instance, peak-locking errors were found to be dependent on the inter-frame time separation by Nogueira *et al* (2011), Legrand *et al* (2012), Adatrao *et al* (2021), among others. Because PIV-UQ algorithms do not account for the systematic error sources or account for them only partly, they give an incomplete or underestimated prediction of the total uncertainty. In order to optimize the PIV data acquisition and processing of a specific experiment, it is crucial to know which experimental factors contribute the most to the uncertainty of the measured velocity fields; however, this information is currently not given by state-of-the-art PIV-UQ approaches.

DOEs is a statistical tool used in many fields of science and engineering to evaluate the systematic effect of input factors on the measurement output (Coleman and Montgomery 1993). The approach was first proposed for wind tunnel measurements by DeLoach (2000) at NASA Langely Research Center due to its various advantages over conventional one factor at a time (OFAT) wind tunnel testing. The chief advantage is that DOE focuses on the generation of adequate prediction models rather than high volume data collection (DeLoach 2000). In a comparison study between OFAT and DOE wind tunnel testing, DeLoach and Micol (2011) showed that the DOE method is more efficient in terms of both resources requirements and ease of data analysis. By using DOE, DeLoach *et al* (2012) were able to quantify the total variance in their wind tunnel measurements and segregate the random and systematic components. The tests were performed in a transonic wind tunnel on a NACA0012 airfoil to compute lift and drag at various angles of attack. The authors found that the systematic component of the variance due to the time variations in sample means was as significant as the ordinary random error. Therefore, the authors concluded that it is important to identify any sources of systematic errors and eliminate them when possible. However, they also highlighted that a residual level of variance is unavoidable, whose systematic component is likely to exceed its random component. An accurate assessment of uncertainty requires that systematic variations be taken into account along with the random variations in the data (DeLoach *et al* 2012).

Aeschliman and Oberkampf (1998) first demonstrated how DOE could be applied to measurement UQ by choosing the bias error sources as factors of interest. Oberkampf and Roy (2010) reported the use of DOE for wind tunnel validation experiments; additionally, they compared the DOE uncertainties with those from the ISO/ANSI method. The authors found that the random component of uncertainty, i.e. uncertainty computed by comparing a large number of replications of the experiment, compare well with the ISO/ANSI approach. However, the total estimated experimental uncertainty using the DOE technique was significantly greater than that estimated by the ISO/ANSI method. With the ISO/ANSI approach, the analyst must make assumptions about which individual uncertainty sources are present as well as the relative magnitudes of those uncertainties and their correlations and interactions. Conversely, in DOE the levels of the related experimental factors are varied to measure the response multiple times such that the main effects of the uncertainty sources as well as their correlations and interactions can be computed rather than assumed.

Smith and Oberkampf (2014) demonstrated that a simplified version of DOE, named error sampling method (ESM), was an alternative tool to overcome the limitations of the traditional PIV-UQ methods. The ESM requires the repetition of an experiment after varying one or more possible sources of errors. In ESM, one seeks to replace as many aspects of the experiment as possible, starting with those that are likely to cause error and that can be varied. By doing so, one is sampling the experimental bias errors, making it possible to quantify the uncertainty due to these contributing error sources. The DOE and ESM techniques provide a means to determine the impact of any variable (i.e. a bias), as well as interaction between the variables (i.e. correlations). In order to do so, one needs to design an experiment in such a way that variations of systematic error sources can be sampled (Smith and Oberkampf 2014).

DeBonis *et al* (2012) made use of a methodology based on DOE to quantify the uncertainty in PIV data for validation of computational fluid dynamics (CFD) simulations. The uncertainties were estimated by comparing the measurements at the intersections of span-wise and stream-wise planes. These comparisons returned not only the uncertainty associated with the statistical convergence of the results, but also a wider range of systematic uncertainties, e.g. due to changes in the laser sheet thickness or interrogation window size. The work showed that the total uncertainty of mean velocity measurements was much larger than that estimated by traditional methods. However, it is to be noticed that the PIV-UQ was conducted only at the intersection lines of the two measurement planes, whereas the uncertainty was not quantified in the rest of the fluid domain. A similar validation experiment using DOE was performed by Rhode and Oberkampf (2012) to assess the predictive accuracy of CFD models for a blunt-body supersonic retro-propulsion configuration at various Mach numbers. The total experimental uncertainty and the constituent uncertainties from a range of sources such as random measurement error, flow field non-uniformity and model/instrumentation asymmetries were successfully evaluated, which were necessary for the validation of the CFD models.

Similarly, Beresh (2009) performed a comparison among the PIV results from multiple experimental configurations and

data processing techniques to quantify the uncertainties associated with the selection of the experimental setup and processing parameters. The data were acquired in the far-field of the interaction between a transverse supersonic jet and a transonic crossflow. The experimental configurations included two-component PIV in the centerline stream-wise plane at two overlapping stations, as well as stereoscopic PIV in both the same stream-wise plane and in the cross plane. Beresh (2009) demonstrated that the bias errors related to calibration and window deformation, which were nontrivial to predict beforehand, dominated the results in the turbulent flow region. This comparison between different PIV configurations and data reduction techniques thus suggests that state-of-the-art methods of UQ may not fully capture all error sources in PIV measurements.

The discussion above shows that the DOE is a valuable tool for quantifying the complete uncertainty (both random and systematic components) of flow measurements, and the contribution of the experimental factors to the uncertainty. In PIV, UQ methods have been proposed that mainly focused on the random uncertainty, which can be retrieved from the data statistics. Approaches based on the ESM or comparisons of different PIV measurements at the same locations showed that PIV uncertainties are potentially significantly larger than those predicted by conventional PIV-UQ approaches because of the presence of systematic error sources. Hence, in this paper, we propose a PIV-UQ approach based on DOE and Analysis of Variances (ANOVA) where the significant experimental factors can be identified along with the systematic uncertainties arising from them. The proposed approach does not aim to replace the established PIV-UQ methodologies such as correlation statistics approach (Wieneke 2015), particle disparity method (Sciacchitano *et al* 2013), uncertainty surface method (Timmins *et al* 2012), cross-correlation peak ratio criterion (Charonko and Vlachos 2013), etc. Rather, it is complementary to them. In fact, these established PIV-UQ methodologies quantify the uncertainty of instantaneous velocity fields, whereas the proposed DOE approach evaluates the uncertainty of statistical flow properties such as time-averaged velocity and Reynolds stresses. Although the DOE approach and the peak ratio and uncertainty surface methods all require the selection of relevant error sources or experimental factors, there is a fundamental difference among these methods: the latter two methods evaluate the uncertainty associated only with the selected error sources. Instead, in the DOE approach, the uncertainty that is not ascribed to the selected experimental factors is evaluated and appears in error term ε (effects of unknown factors) as explained in section 2. As the proposed approach allows to evaluate the uncertainty of systematic error sources and to quantify their contributions to the total uncertainty, it can be used to optimize experiments and minimize the overall uncertainty. Moreover, the approach is comprehensive in that it can be applied universally, irrespective of the kind of PIV setup, e.g. planar PIV, tomographic particle tracking velocimetry (PTV), large scale PIV or microscopic PTV, for UQ in any of the measured quantities, e.g. mean velocity or higher order statistics. The proposed methodology is described in section 2. The approach is experimentally assessed for planar PIV measurements of the flow over a NACA0012 airfoil in a wind tunnel. The experimental setup and results of the UQ in mean velocity and Reynolds stress are presented in section 3. Moreover, the methodology is applied to a stereoscopic PIV experiment dealing with the flow at the outlet of a ducted Boundary Layer Ingesting (BLI) propulsor. The results of this application are briefly shown in section 4.

2. Design of experiments and ANOVA

DOE refers to the process of planning the experiment in order to collect appropriate data that can be analyzed by statistical methods resulting in valid and objective conclusions (Montgomery 2013). In any experiment, some of the experimental parameters directly affect the output value and are called *design factors*; in PIV measurements, those are for instance the inter-frame time separation, interrogation window size, camera aperture, laser sheet thickness, etc. Additionally, some of the parameters, which affect the output directly or indirectly (in combination with the design factors) but are uncontrollable or only partly controllable during the measurements, are called *nuisance factors*; for PIV, those include variations of the fluid properties during a measurement, seeding density and its distribution, etc. Different measurements of an ideally constant quantity with varying levels of the design and/or nuisance factors show variations in the measured quantity. A proper data acquisition model and statistical analysis can be used to quantify the variance in the output quantity due to the variations in the levels of input factors and their combinations.

The present work employs the statistical tools DOE and ANOVA to quantify the total uncertainty and the contribution of the design and nuisance factors to the total uncertainty. Following Montgomery (2013), a randomized complete block design is considered for data acquisition, as *blocking* is necessary for tackling the effect of the nuisance factors; in such experimental design, measurements are carried out in two or more blocks (or levels of the nuisance factor) and levels of the design factors are varied randomly in each block. The analysis can be performed by choosing as many factors as one is interested in. However, the number of measurement runs increases with the number of factors and their levels as L^N, being N the number of experimental factors and L the number of levels of each factor (assumed to be the same for all factors). Let us take an example of experiment with two design factors A and B with a and b number of levels, respectively, and one blocking factor with n number of levels. Following Montgomery (2013), a linear statistical model for this design is:

$$y_{ijk} = \mu + A_i + B_j + (AB)_{ij} + \text{Block}_k + \varepsilon_{ijk}, \qquad (1)$$

where, y_{ijk} is the observed response at the ith level of factor A and jth level of factor B in kth block, μ is the overall mean effect, A_i is the effect of the ith level of factor A, B_j is the effect of the jth level of factor B, $(AB)_{ij}$ is the effect of the interaction between A_i and B_j, Block_k is the effect of the kth level of the blocking factor, and ε_{ijk} is an error component consisting of

Table 1. Analysis of Variances (ANOVA) table for Two-Factor Randomized Complete Block Design (RCBD).

Source	Sum of Squares	Degrees of Freedom	Mean Squares	F_0
A	$\mathrm{SS}_A = \frac{1}{bn}\sum_{i=1}^{a} y_{i..}^2 - \frac{y_{...}^2}{abn}$	$a-1$	$\mathrm{MS}_A = \frac{\mathrm{SS}_A}{a-1}$	$F_0 = \frac{\mathrm{MS}_A}{\mathrm{MS}_\varepsilon}$
B	$\mathrm{SS}_B = \frac{1}{an}\sum_{j=1}^{b} y_{.j.}^2 - \frac{y_{...}^2}{abn}$	$b-1$	$\mathrm{MS}_B = \frac{\mathrm{SS}_B}{b-1}$	$F_0 = \frac{\mathrm{MS}_B}{\mathrm{MS}_\varepsilon}$
AB	$\mathrm{SS}_{AB} = \frac{1}{n}\sum_{i=1}^{a}\sum_{j=1}^{b} y_{ij.}^2 - \frac{y_{...}^2}{abn} - \mathrm{SS}_A - \mathrm{SS}_B$	$(a-1)(b-1)$	$\mathrm{MS}_{AB} = \frac{\mathrm{SS}_{AB}}{(a-1)(b-1)}$	$F_0 = \frac{\mathrm{MS}_{AB}}{\mathrm{MS}_\varepsilon}$
Block	$\mathrm{SS}_{\mathrm{Block}} = \frac{1}{ab}\sum_{k=1}^{n} y_{..k}^2 - \frac{y_{...}^2}{abn}$	$n-1$	$\mathrm{MS}_{\mathrm{Block}} = \frac{\mathrm{SS}_{\mathrm{Block}}}{n-1}$	$F_0 = \frac{\mathrm{MS}_{\mathrm{Block}}}{\mathrm{MS}_\varepsilon}$
E	$\mathrm{SS}_\varepsilon = \mathrm{SS}_{\mathrm{Total}} - \mathrm{SS}_A - \mathrm{SS}_B - \mathrm{SS}_{AB} - \mathrm{SS}_{\mathrm{Block}}$	$(ab-1)(n-1)$	$\mathrm{MS}_\varepsilon = \frac{\mathrm{SS}_\varepsilon}{(ab-1)(n-1)}$	
Total	$\mathrm{SS}_{\mathrm{Total}} = \sum_{i=1}^{a}\sum_{j=1}^{b}\sum_{k=1}^{n} y_{ijk}^2 - \frac{y_{...}^2}{abn}$	$abn-1$	$\mathrm{MS}_{\mathrm{Total}} = \frac{\mathrm{SS}_{\mathrm{Total}}}{abn-1}$	

random error and the effect of unknown factors in the measurements. For this model, we are interested in checking whether the effects A_i, B_j, $(AB)_{ij}$ and Block_k are zero (*null hypothesis*) or non-zero (*alternative hypothesis*). This can be achieved by the factorial ANOVA (Montgomery 2013) as shown in table 1, where $y_{i.}$ denotes the total of all observations under the ith level of factor A, $y_{.j}$ denotes the total of all observations under the jth level of factor B, y_{ij} denotes the total of all observations under the ith level of factor A and jth level of factor B, $y_{.k}$ denotes the total of all observations under the kth level of blocking factor, and $y_{..}$ denotes the grand total of all the observations. These terms can be expressed mathematically as:

$$y_{i..} = \sum_{j=1}^{b}\sum_{k=1}^{n} y_{ijk}, y_{.j.} = \sum_{i=1}^{a}\sum_{k=1}^{n} y_{ijk}, y_{ij.} = \sum_{k=1}^{n} y_{ijk},$$
$$y_{..k} = \sum_{i=1}^{a}\sum_{j=1}^{b} y_{ijk}, y_{...} = \sum_{i=1}^{a}\sum_{j=1}^{b}\sum_{k=1}^{n} y_{ijk}. \quad (2)$$

From ANOVA table 1, the significance of the factor effects is determined by performing F-test with desired confidence level, where the F_0 values are computed as the ratios of the mean squares (MS) of the effects to the error mean square (MS_ε). The F_0 values are then compared with a critical value F_c based on the desired confidence level and degrees of freedom of the factors. If the F_0 value is greater than F_c, then the corresponding effect is statistically significant with the desired level of confidence, and the null hypothesis shall be rejected. The reader is referred to any standard book on statistics for a detailed explanation of the F-test (for example, Montgomery 2013). It is thus possible to segregate the contribution of every factor in the total variance of the measurement. The total uncertainty (U_{Total}) and constituent systematic uncertainties (U_X) in the response variable are calculated as:

$$U_{\mathrm{Total}} = \sqrt{\frac{\mathrm{SS}_{\mathrm{Total}}}{abn-1}} = \sqrt{U_A^2 + U_B^2 + U_{AB}^2 + U_{\mathrm{Block}}^2 + U_\varepsilon^2} \quad (3)$$

$$U_X = \sqrt{\frac{\mathrm{SS}_X}{abn-1}} \text{ and } X = A, B, AB, \mathrm{Block}, \varepsilon, \quad (4)$$

where SS is the sum of squares and represents the variability in the response variable as shown in table 1.

3. Experimental assessment

The proposed methodology was assessed for planar PIV measurements of the flow over a NACA0012 airfoil at 15 degrees angle of attack. For sake of limiting the times for data acquisition and processing, we considered only four design factors, namely camera aperture, inter-frame time separation, interrogation window size, laser sheet thickness and one blocking factor of seeding density. The total uncertainties as well as the constituent systematic uncertainties due to the five factors were quantified for the measured time-averaged velocity and Reynolds stress.

3.1. Experimental setup

The planar PIV measurements were performed for the flow over a NACA0012 airfoil where the experimental setup was similar to that of the measurements conducted by Adatrao *et al* (2021). Figure 1 illustrates a schematic of the experimental setup.

The experiment was conducted in the W-tunnel of Delft University of Technology. This open-jet open-return wind tunnel has an exit cross section of 0.4 × 0.4 m^2 and an area contraction ratio of 9. The maximum achievable free-stream velocity is 30 m s^{-1} with 0.3% turbulence intensity (Tummers 1999). In this experiment, the free stream velocity was set to 10 m s^{-1}. The flow was seeded by a SAFEX seeding generator, which produces water-glycol droplets of 1 μm median diameter. The particles were illuminated by a Quantel Evergreen 200 laser (Nd:YAG, pulse energy of 200 mJ per pulse, wavelength of 532 nm) and images were recorded with a LaVision Imager sCMOS camera (12 bits, 6.5 μm pixel size, 2560 × 2160 pixels maximum resolution) with image sensor cropped to 2240 × 1622 pixels. The camera was equipped with a Nikon objective of 105 mm focal length and a field of view (FOV) of 135 mm × 98 mm was imaged with optical magnification of 0.11. The aim of this experimental assessment was to employ the statistical tools DOE and ANOVA to quantify the total uncertainty in time-averaged PIV measurements and the contribution of the design and nuisance factors to the total uncertainty. Various factors during the acquisition and processing stages contribute to the total uncertainty.

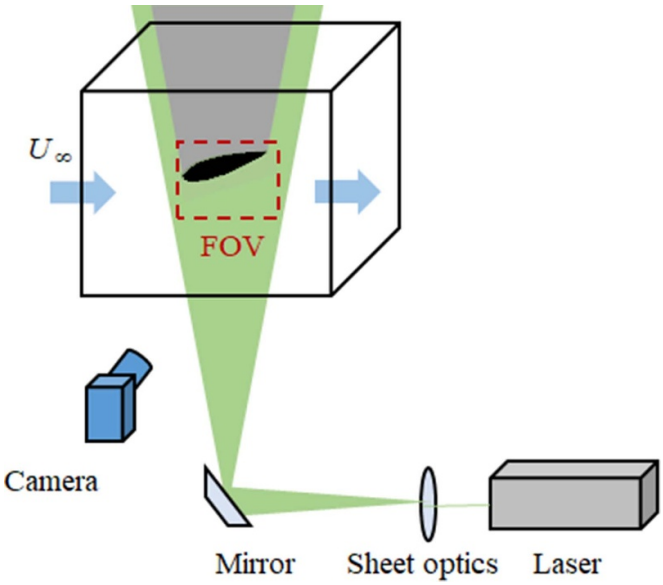

Figure 1. Schematic experimental setup of the planar PIV measurements of the flow over a NACA0012 airfoil at 15 degrees angle of attack.

However, only some of the most important ones are considered for the analysis. Following Scharnowski *et al* (2019), five factors, namely camera aperture ($f\#$), inter-frame time separation (Δt), interrogation window size (D_I), laser sheet thickness (Δz) and seeding density were considered to be the most relevant. Therefore, for the analysis four design factors $f\#$, Δt, D_I, Δz (assigned with *A, B, C, D*, respectively) and a blocking factor (seeding density) with two levels of each were selected. The two levels of the factors are: $f\# = 4$ and 8, $\Delta t = 50$ and 70 μs [resulting displacements in the free stream ($U_\infty = 10$ m s^{-1}) are 8.5 and 11.8 pixels, respectively], $D_\mathrm{I} = 16 \times 16$ and 64×64 pixels (0.95×0.95 and 3.78×3.78 mm in physical units), $\Delta z = 1$ and 3 mm, and seeding density = 0.01 ppp–0.02 ppp and 0.08 ppp–0.09 ppp (resulting in mean particle distances of 0.2 and 0.5 mm, respectively), as summarised in table 2. Following the 2^N rule, N being the number of design factors, a total of 32 measurements were performed ($2^4 = 16$ in each block). The images were recorded and processed using LaVision Davis10 software. The data set at each run consisted of 1000 double-frame images and a total of 16 runs per block were performed in a random order. Each measurement run was unique corresponding to the combination of one of the two levels of the four design factors. The processing was done using Gaussian interrogation windows of 128×128 pixels with 75% overlap for the initial passes and 16×16 pixels or 64×64 pixels with 75% overlap for the final passes.

The estimated time-averaged stream-wise velocity component u and in-plane velocity vectors are shown in figure 2; the measured Reynolds normal stresses R_{uu} are shown in figure 3. It is to be noted that figures 2 and 3 show the values averaged over all 32 measurement runs. It is clear that the flow has varying degrees of fluctuations, e.g. low fluctuations in the potential flow region ($0.01 < R_{uu} < 0.1$ m^2 s^{-2}) and relatively high fluctuations in the separated shear layer and the turbulent wake ($5 < R_{uu} < 8$ m^2 s^{-2}). Therefore, the measured flow field is a suitable case to implement and assess the feasibility of the proposed approach in a range of flow conditions encountered in typical PIV measurements. The analysis was performed for the whole FOV to quantify the total uncertainties in the time-averaged velocities and Reynolds stresses and the contribution of the individual factors to the total uncertainties. However, for simplicity, two points were chosen in two different regions based on the amount of flow fluctuations, as shown in figure 3, to explain the contribution of the factors to the total uncertainties. The results at these two points are explained in detail in section 3.2.

Table 2. Factors and their levels in the planar PIV measurements of the flow over a NACA0012 airfoil.

Factor	Parameter	Levels
A	$f\#$	4, 8
B	Δt	50, 70 μs
C	D_I	16×16, 64×64 pixels (0.95×0.95, 3.78×3.78 mm)
D	Δz	1, 3 mm
Block	Seeding density	0.01–0.02, 0.08–0.09 ppp (mean particle distances of 0.2 and 0.5 mm)

3.2. Results

3.2.1. Uncertainty of mean velocity. The total uncertainties of the mean or time-averaged stream-wise velocities were calculated following equation (3) and are shown in figure 4(a). As expected, the uncertainties estimated by the DOE approach are higher than the random uncertainties calculated from data statistics for a specific run (the considered case is: $f\# = 8$, $\Delta t = 50$ μs, $D_\mathrm{I} = 16 \times 16$ pixels, $\Delta z = 1$ mm and seeding density = 0.08–0.09 ppp) as $\sigma/\sqrt{N_\mathrm{s}}$ (see figure 4(b)), with σ the standard deviation and N_s the number of samples (Sciacchitano and Wieneke 2016). It is clear that the random uncertainties from data statistics are underestimated as the systematic effects of the experimental factors are not taken into consideration. The methodology based on DOE, on the other hand, is able to compute the systematic contributions of the factors considered in the analysis to the total uncertainty. Nevertheless, the random uncertainty of the mean velocity is proportional to the flow fluctuations or Reynolds stress values. Moreover, larger total uncertainty is retrieved in the regions of high velocity gradients, as reported by Scarano (2002), which are mainly encountered in the shear layer. Following these observations, a detailed analysis of the constituent systematic uncertainties is made at points I and II, located in the potential flow region and turbulent region, respectively (see figure 3).

The ANOVA results at the two selected points were obtained in the form of table 3, where the F_0 values corresponding to the main and interaction effects of the design and blocking factors are calculated as shown in the last column in table 1. The F-test is then performed to estimate whether the effects are statistically significant or not, which is done

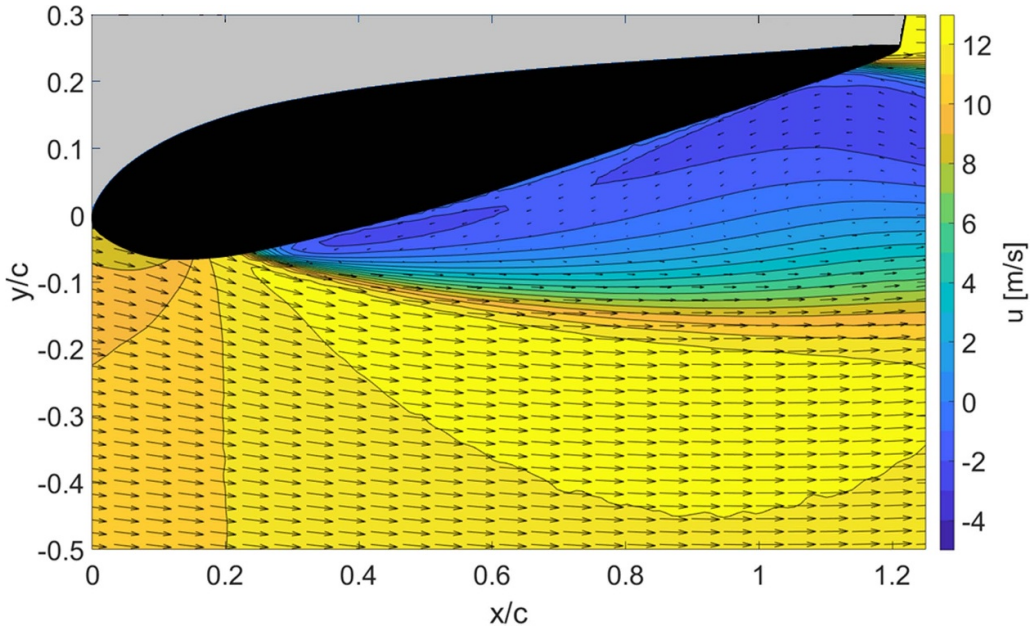

Figure 2. Measured time-averaged stream-wise velocity component u and in-plane velocity vectors (averaged over 32 measurement runs).

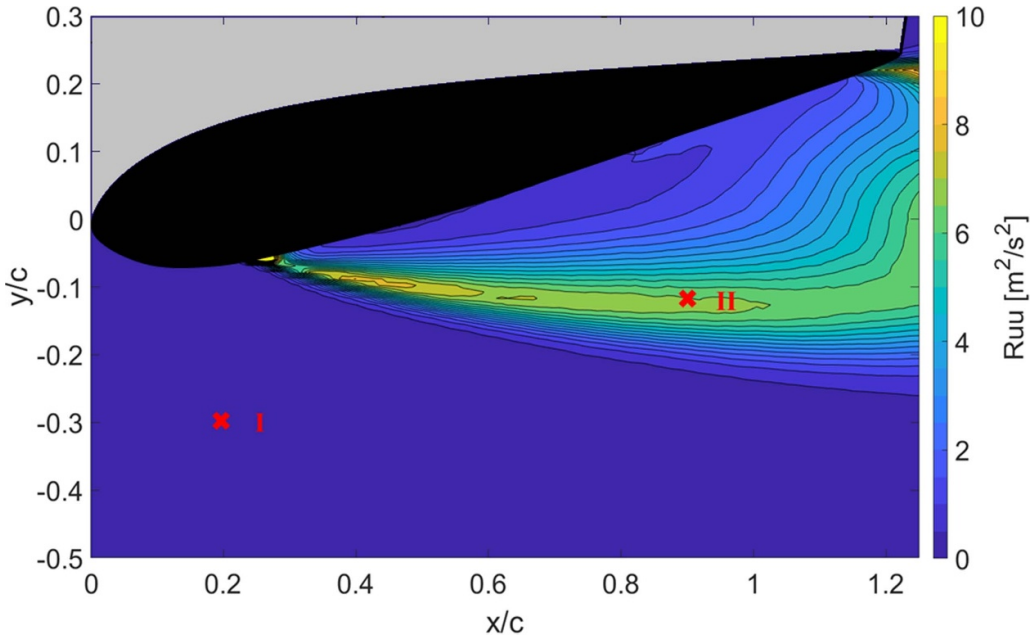

Figure 3. Reynolds normal stresses averaged over 32 measurement runs (The results of application of the proposed approach are shown in detail in section 3.2 at points I and II).

by comparing the F_0 values with the critical value F_c that, in the present case (for 1 degree of freedom of numerator and 20 degrees of freedom of denominator), is 4.35 for 95% confidence level (Montgomery 2013). If the F_0 value is greater than F_c, then the corresponding effect is statistically significant with the desired level of confidence. For example, for the point I, the main effect of factor B (i.e. Δt) is statistically significant as it yields an F_0 value of 40.17. Instead, at point II, where the flow fluctuations are larger, factor D (i.e. the laser sheet thickness Δz) has a statistically significant effect, leading to an F_0 value of 6.81. At both points I and II, as in most of the measurement domain, the effect of the seeding density (block) is statistically significant, because it directly affects the valid detection probability as reported by Scharnowski *et al* (2019). Instead, the other experimental factors (factors *A, C* and *D* at point I; factors *A, B, C* at point II) as well as the interaction effects between the factors do not have a statistically significant effect on the total uncertainty.

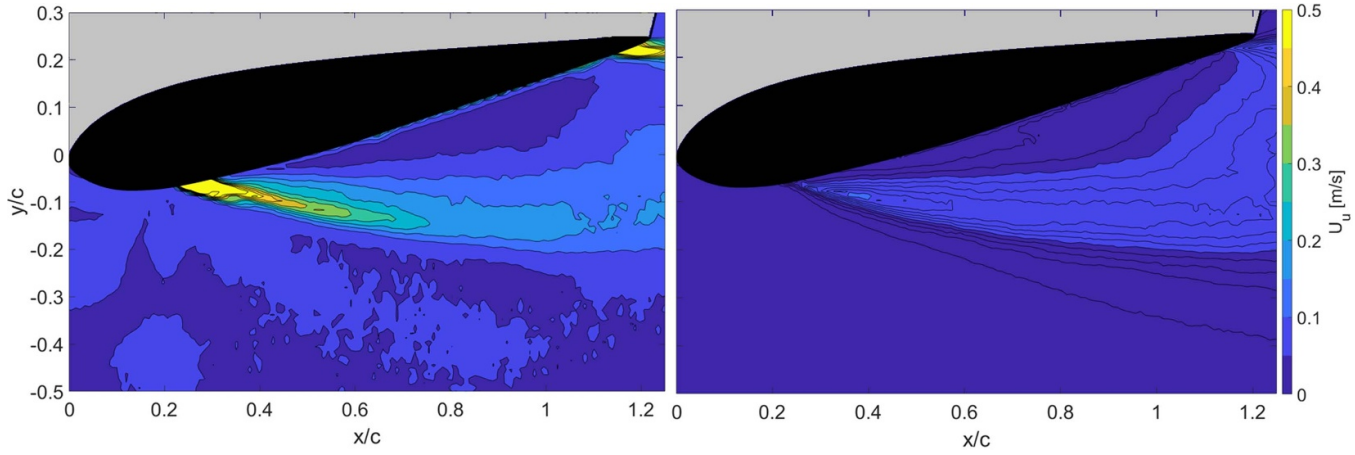

(a) total uncertainty by proposed methodology based on DOE

(b) random uncertainty from data statistics $(\sigma/\sqrt{N_s})$

Figure 4. Uncertainty in time-averaged stream-wise velocity u.

Table 3. Analysis of Variances (ANOVAs) results in the uncertainty quantification of mean stream-wise velocity u where *A, B, C, D* and Block correspond to the factors: camera aperture $f\#$, inter-frame time separation Δt, interrogation window size D_I, laser sheet thickness Δz and seeding density, respectively (The critical value $F_\mathrm{c} = 4.35$ for 1 degree of freedom of numerator and 20 degrees of freedom of denominator at 95% confidence level (Montgomery 2013)).

		Point I				Point II			
Source	Degrees of Freedom	Sum of Squares ($m^2\ s^{-2}$)	Mean Squares ($m^2\ s^{-2}$)	F_0	U_X ($m\ s^{-1}$)	Sum of Squares ($m^2\ s^{-2}$)	Mean Squares ($m^2\ s^{-2}$)	F_0	U_X ($m\ s^{-1}$)
A ($f\#$)	1	0.0026	0.0026	3.98	0.0092	0.0000	0.0000	0.00	0.0008
B (Δt)	1	0.0264	0.0264	**40.17**	0.0292	0.0006	0.0006	0.04	0.0042
C (D_I)	1	0.0000	0.0000	0.06	0.0011	0.0099	0.0099	0.68	0.0178
D (Δz)	1	0.0003	0.0003	0.40	0.0029	0.0995	0.0995	**6.81**	0.0566
AB	1	0.0028	0.0028	4.27	0.0095	0.0017	0.0017	0.12	0.0074
AC	1	0.0000	0.0000	0.00	0.0002	0.0034	0.0034	0.23	0.0104
AD	1	0.0000	0.0000	0.01	0.0004	0.0241	0.0241	1.65	0.0279
BC	1	0.0000	0.0000	0.01	0.0005	0.0016	0.0016	0.11	0.0071
BD	1	0.0002	0.0002	0.34	0.0027	0.0000	0.0000	0.00	0.0005
CD	1	0.0000	0.0000	0.01	0.0005	0.0039	0.0039	0.27	0.0112
Block	1	0.0246	0.0246	**37.38**	0.0282	0.1896	0.1896	**12.99**	0.0782
ε	20	0.0131	0.0007	—	0.0206	0.2921	0.0146	—	0.0971
Total	31	0.0701	0.0023	—	0.0476	0.6262	0.0202	—	0.1421

The constituent uncertainties due to the main and interaction effects of the factors were calculated by equation (4) and are reported in the last column of table 3. Their contributions to the total uncertainty in the stream-wise velocity u are shown in the form of pie charts in figure 5. It is to be noted that the percentage contributions were calculated for the squares of the individual uncertainties as they add to the square of the total uncertainty (see equation (3)). The sub-figures (a) and (b) are for the points I and II, respectively, which are marked in figure 3. The mean stream-wise velocity (u) components at these points are 11.02 m s^{-1} and 4.58 m s^{-1}, respectively. The corresponding total uncertainties are 0.05 m s^{-1} and 0.14 m s^{-1}, which are shown in the centre of the pie charts in figure 5.

It is clear that the total uncertainty increases with increase in the velocity gradient and the flow fluctuations, which agrees with the observation in the contour plot of total uncertainty in figure 4. The seeding density (block) contributes to around 35% and 30% to the total uncertainty in the time-averaged stream-wise velocity at the points I and II, respectively. The factor *B*, i.e. inter-frame time separation Δt, is the most significant factor at point I and contributes to 38% of the total uncertainty. At this point, where the flow fluctuations are very low and the mean velocity is largely affected by peak-locking errors, the factor Δt influences directly the magnitude of peak-locking errors the most, as observed by Legrand *et al* (2012).

At the point II, i.e. in the flow region of high flow fluctuations, apart from the seeding density, the factor *D* i.e. laser

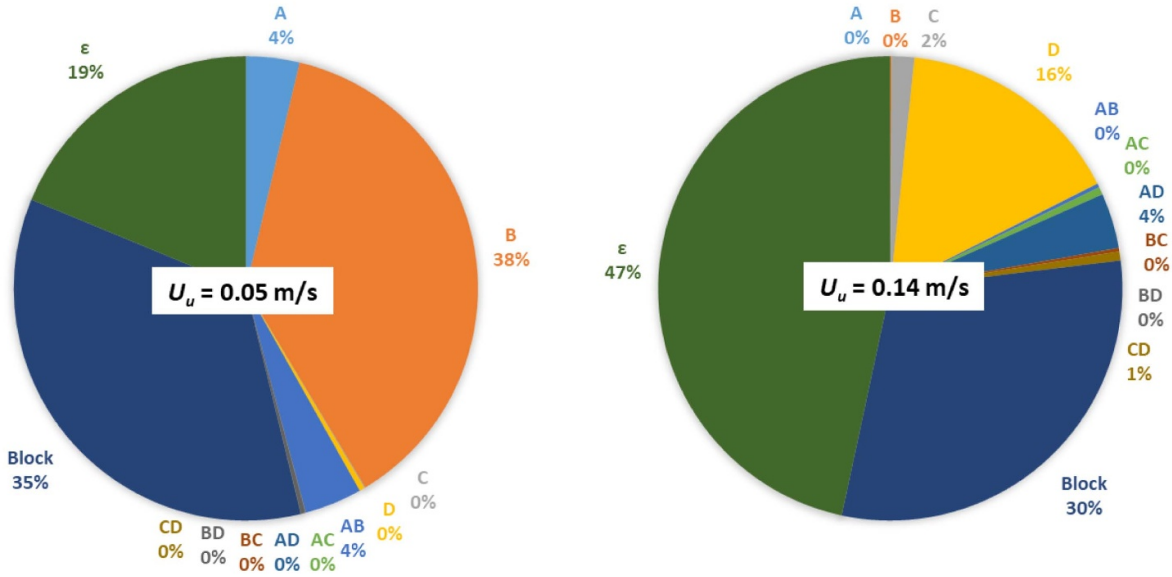

(a) Point I (potential flow region) (b) Point II (turbulent region)

Figure 5. Contribution of systematic uncertainties to the total uncertainty in time-averaged stream-wise velocity at the two points marked in figure 3, due to main and interaction effects of the factors: A (camera aperture $f\#$), B (inter-frame time separation Δt), C (interrogation window size D_I), D (laser sheet thickness Δz) and block of seeding density.

sheet thickness Δz is statistically significant and contributes to 16% of the total uncertainty of the time-averaged stream-wise velocity as shown in the pie chart in figure 5(b). This is due to the three-dimensional nature of the flow in the turbulent region of the flow, thus the larger value of Δz may cause a larger dispersion of the particles displacements within the interrogation window. Moreover, the random error (factors not directly considered in the analysis, e.g. limited statistical convergence, image noise, etc) shows significant contribution of 47% to the total uncertainty. This is due to the flow fluctuations in these regions being high which, owed to the limited statistical convergence of the measurements, makes it difficult to segregate the contribution of individual systematic uncertainties. It is to be noted that the '*error uncertainty* ε' from the ANOVA represents the random uncertainty in the measurements plus the uncertainty due to the unknown experimental factors (i.e. the factors not considered as design or blocking factors). The effect of the factor C (interrogation window size D_I) is not statistically significant at the points I and II. However, in high-shear regions of the flow, it contributes significantly to the total uncertainty of the mean stream-wise velocity (the results are not shown for conciseness).

3.2.2. Uncertainty of Reynolds stress. The proposed methodology was also applied for UQ of the higher order statistics such as the Reynolds stresses. The equations (3) and (4) were used to calculate the total uncertainty and the constituent systematic uncertainties, respectively. The estimated total uncertainties of the Reynolds normal stresses are shown in figure 6(a). As seen for the total uncertainty of the mean stream-wise velocity, also the total uncertainties of the Reynolds normal stresses are the highest in the regions of high flow fluctuations. These total uncertainties estimated by the proposed DOE approach are compared to random uncertainties calculated from data statistics. Figure 6(b) shows the random uncertainties in a single run ($f\# = 8$, $\Delta t = 50$ µs, $D_\mathrm{I} = 16 \times 16$ pixels, $\Delta z = 1$ mm and seeding density = 0.08 ppp–0.09 ppp) calculated as $R_{uu}\sqrt{\frac{2}{N_\mathrm{s}-1}}$, with R_{uu} the Reynolds normal stress and N_s the number of samples (Sciacchitano and Wieneke 2016). It is clear that the random uncertainties are highly underestimated as the systematic effects of the experimental factors are not taken into consideration, as was also shown for the uncertainty of mean velocity in section 3.2.1.

Two points in two flow regions were selected as marked in figure 3 to evaluate the results for the constituent systematic uncertainties based on the amount of flow fluctuations. The results of ANOVA tests for these two points can be seen in table 4, and the pie charts in figure 7 show the contribution of the main and interaction effects of the design and blocking factors to the total uncertainty. The average Reynolds normal stresses at the points I and II are 0.01 and 5.99 $\mathrm{m^2\ s^{-2}}$, respectively, and the corresponding total uncertainties are 0.008 and 0.65 $\mathrm{m^2\ s^{-2}}$, which are shown in the centre of pie charts in figure 7. It is clear that the total uncertainty increases with increase in the flow fluctuations, which agrees with the observation in the contour plot of total uncertainty in figure 6. In most of the measurement domain, the main effects of the factor C (interrogation window size D_I) and the seeding density (block) are statistically significant, whereas all the two-way interaction effects are found to be insignificant, as also observed in the measurement of the mean stream-wise velocities. The seeding density directly affects the valid detection probability (Scharnowski *et al* 2019) and thus has a significant

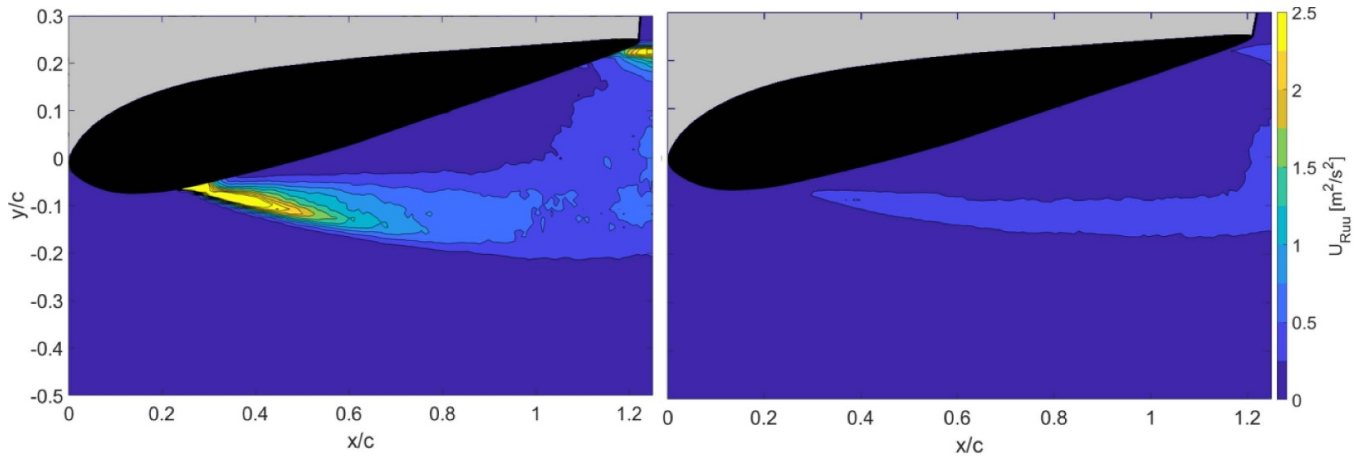

(a) total uncertainty by proposed methodology based on DOE

(b) random uncertainty from data statistics $(R_{uu}\sqrt{\frac{2}{N_s-1}})$

Figure 6. Uncertainty in Reynolds normal stress R_{uu}.

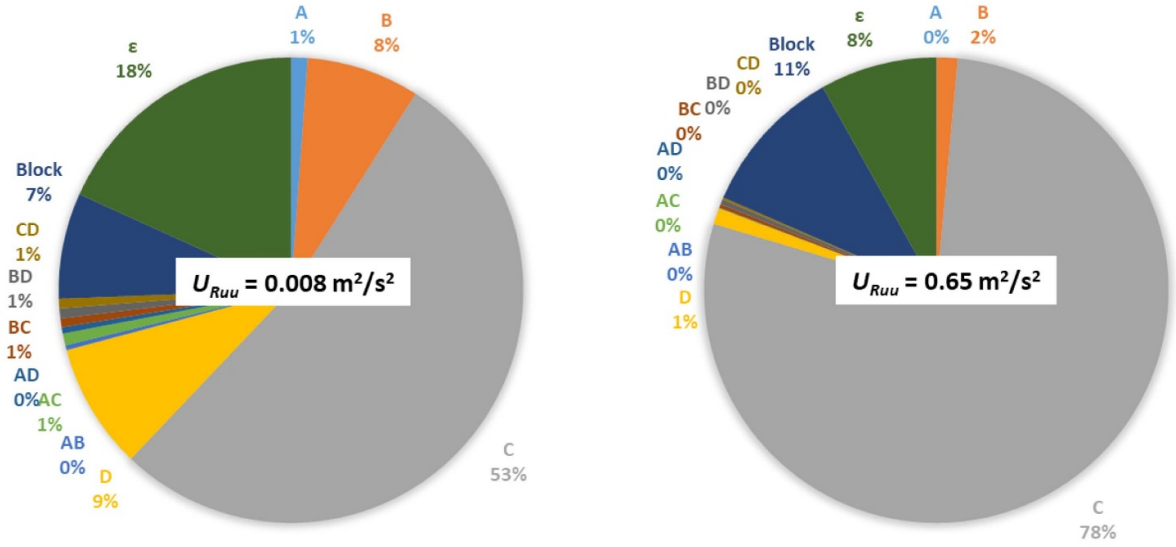

(a) Point I (potential flow region)

(b) Point II (turbulent region)

Figure 7. Contribution of systematic uncertainties to the total uncertainty in Reynolds normal stress at the two points marked in figure 3, due to main and interaction effects of the factors- *A* (camera aperture *f*#), *B* (inter-frame time separation Δt), *C* (interrogation window size D_I), *D* (laser sheet thickness Δz) and block of seeding density.

effect on the measurement uncertainty. It contributes to around 7% and 11% of the total uncertainty in the Reynolds normal stress at the points I and II, respectively. As shown in table 4 and figure 7, the factor *C* interrogation window size D_I is the most significant at both the points and contributes to 53% and 78% of the total uncertainty at the points I and II, respectively. Moreover, the factors *B* and *D*, i.e. inter-frame time separation Δt and laser sheet thickness Δz, are also statistically significant at the point I in the potential flow region. They contribute to 8% and 9% of the total uncertainty, respectively.

4. Application to BLI propulsor flow

The proposed methodology was applied to a wind tunnel experiment of a ducted BLI propulsor.

4.1. Experimental setup

The experiment was conducted in the low-speed tunnel operated by the German-Dutch Wind Tunnels. The measurements were performed at a Mach number of 0.174 and a body

Table 4. Analysis of Variances (ANOVA) results in the uncertainty quantification of Reynolds normal stress R_{uu} where *A, B, C, D* and Block correspond to the factors: camera aperture $f\#$, inter-frame time separation Δt, interrogation window size D_I, laser sheet thickness Δz and seeding density, respectively (The critical value $F_\mathrm{c} = 4.35$ for 1 degree of freedom of numerator and 20 degrees of freedom of denominator at 95% confidence level (Montgomery 2013)).

		Point I				Point II			
Source	Degrees of Freedom	Sum of Squares ($m^4\ s^{-4}$)	Mean Squares ($m^4\ s^{-4}$)	F_0	U_X ($m^2\ s^{-2}$)	Sum of Squares ($m^4\ s^{-4}$)	Mean Squares ($m^4\ s^{-4}$)	F_0	U_X ($m^2\ s^{-2}$)
A ($f\#$)	1	0.0000	0.0000	1.26	0.0008	0.0038	0.0038	0.07	0.0111
B (Δt)	1	0.0002	0.0002	**8.62**	0.0022	0.1849	0.1849	3.57	0.0772
C (D_I)	1	0.0010	0.0010	**58.20**	0.0057	9.9625	9.9625	**192.17**	0.5669
D (Δz)	1	0.0002	0.0002	**9.60**	0.0023	0.1418	0.1418	2.73	0.0676
AB	1	0.0000	0.0000	0.37	0.0005	0.0002	0.0002	0.00	0.0026
AC	1	0.0000	0.0000	0.90	0.0007	0.0069	0.0069	0.13	0.0149
AD	1	0.0000	0.0000	0.49	0.0005	0.0000	0.0000	0.00	0.0004
BC	1	0.0000	0.0000	0.67	0.0006	0.0339	0.3394	0.65	0.0331
BD	1	0.0000	0.0000	0.75	0.0006	0.0442	0.0442	0.85	0.0378
CD	1	0.0000	0.0000	0.74	0.0007	0.0178	0.0178	0.34	0.0240
Block	1	0.0001	0.0001	**8.04**	0.0021	1.3195	1.3195	**25.45**	0.2063
E	20	0.0003	0.0000	—	0.0034	1.0368	0.0518	—	0.1829
Total	31	0.0021	0.0001	—	0.0083	13.0577	0.4212	—	0.6490

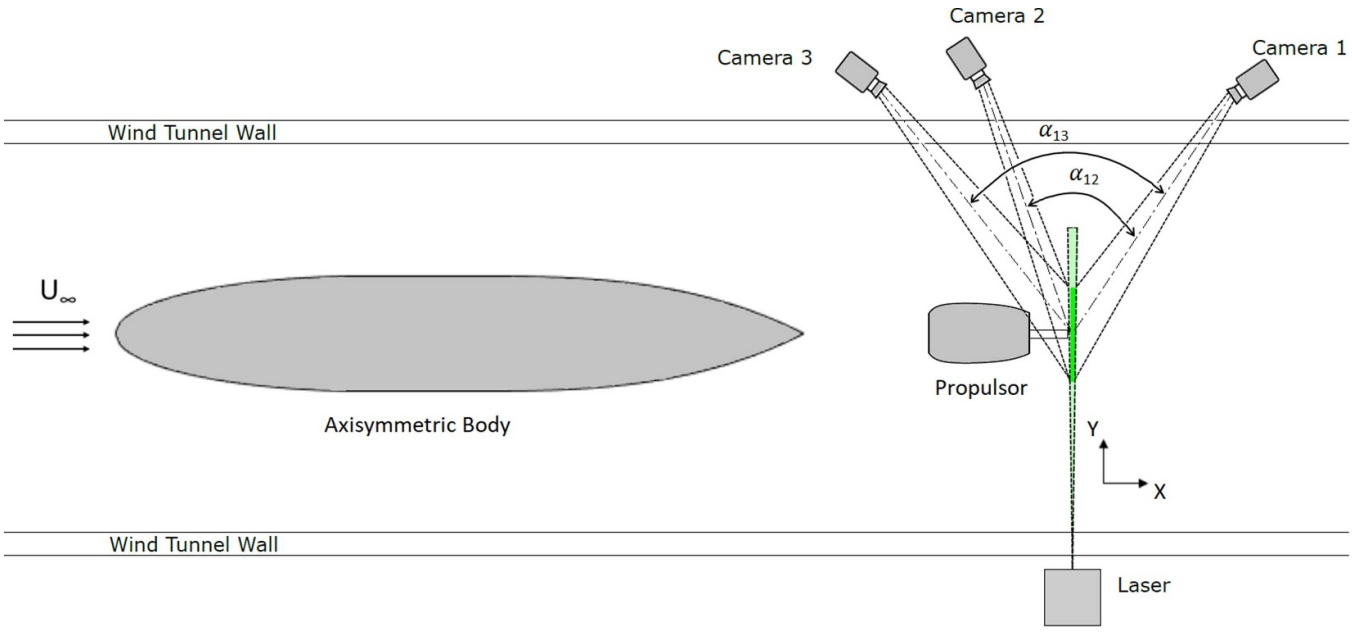

Figure 8. Schematic experimental setup of stereoscopic PIV measurements at the outlet of the ducted Boundary Layer Ingesting (BLI) propulsor.

length-based Reynolds number of 6×10^6 corresponding to a freestream velocity (U_∞) of 60 m s^{-1}. The test case consisted of an axisymmetric body placed upstream of the propulsor as shown in figure 8, where stereoscopic PIV measurements were performed in a cross plane at the outlet of the propulsor.

In this experimental campaign, we employed the statistical tools DOE and ANOVA to quantify the total uncertainty in time-averaged velocities and the contribution of the design and nuisance factors to the total uncertainty. Following Sciacchitano (2019) and Bhattacharya *et al* (2016), among others, three design factors, namely camera aperture ($f\#$), inter-frame time separation (Δt) and interrogation window size (D_I), assigned with *A, B, C*, respectively, and one blocking factor of stereoscopic camera angle (α) were selected for the analysis. Two measurement levels were considered for each factor, which are reported in table 5. Following the 2^N rule, *N*

Table 5. Factors and their levels in the stereoscopic PIV measurements at the outlet of the ducted Boundary Layer Ingesting (BLI) propulsor.

Factor	Parameter	Levels
A	$f\#$	4, 5.6
B	Δt	16, 20 μs
C	D_I	16 × 16, 32 × 32 pixels
Block	A	44, 54 degrees

being the number of design factors, a total of 16 measurements were performed ($2^3 = 8$ in each block).

Three LaVision Imager sCMOS cameras were used to perform the measurements with two different stereoscopic angles (i.e. in two blocks). The cameras 1 and 2 formed the stereoscopic angle (α_{12}) of 44° and were considered to be the block I, whereas the cameras 1 and 3 formed the stereoscopic angle (α_{13}) of 54° and were considered to be the block II. It is to be noted that stereoscopic angles larger than 60° are often employed in stereo-PIV measurements. However, in the present experiments, the camera angles were limited by limitations on the optical access. The cameras were mounted with objective lenses of 135 mm focal length and Scheimpflug adapter. The FOV obtained was 260 mm × 220 mm and the values of magnification factors averaged over the entire FOV for the cameras 1, 2 and 3 were 0.067, 0.073 and 0.069, respectively. The flow was seeded by an aerosol seeding generator, which produces DEHS droplets of 1 μm median diameter. The particles were illuminated by a Quantel Evergreen 200 laser (Nd:YAG, pulse energy of 200 mJ per pulse, wavelength of 532 nm) forming a sheet of 4 mm thickness. The images were recorded and processed using the LaVision Davis10 software. The data set at each run consisted of 2000 double-frame images and a total of 8 runs per block (stereoscopic camera angle) were performed in a random order. The geometric stereoscopic calibration via the pinhole model (Prasad 2000) was followed by the self-calibration based on particle images (Wieneke 2005). The processing was done using Gaussian interrogation windows of 64 × 64 pixels with 50% overlap for the initial passes and 16 × 16 pixels or 32 × 32 pixels with 50% overlap for the final passes.

4.2. Results

The estimated time-averaged stream-wise velocity component u and in-plane (Y–Z plane) velocity vectors are shown in figure 9. The wake region can be seen in the centre of the measurement domain, whereas the outer region represents potential flow with stream-wise velocity of 60 m s^{-1}. The flow is retarded at the periphery of the propulsor and the discontinuities in the mean stream-wise velocity field due to the stator ring can be seen at the periphery. Moreover, the in-plane velocity vectors are shown in figure 9 illustrating the magnitude and direction of Y and Z-velocity components v and w, respectively. The counter-clockwise rotation of the flow in the wake of the propulsor can be easily seen due to the direction of the vectors, where the magnitudes of v and w velocity components are larger than those in the outer potential flow region. The contour plot of the total uncertainty (U_u) of the mean stream-wise velocity component u is shown in figure 10. The total uncertainty of the mean velocity closely resembles the fluctuations root-mean-square, as was also observed in the experimental assessment with NACA0012 airfoil. Moreover, the outer edge of the propulsor slipstream exhibits larger total uncertainty due to high velocity gradients in this region.

To explain the contribution of the individual factors to the total uncertainty, three points in three different flow regions were chosen based on the amount of flow fluctuations and velocity gradients, as marked in figure 11. The points I, II and III correspond to the potential flow region, shear layer and jet region, respectively. The mean stream-wise velocity (u) components at these points are 59.20 m s^{-1}, 64.17 m s^{-1} and 59.75 m s^{-1}, respectively and the corresponding total uncertainties are 0.37 m s^{-1}, 1.60 m s^{-1} and 0.51 m s^{-1}. It is clear that the total uncertainty increases with increase in the velocity gradient and the flow fluctuations, which agrees with the observation in the contour plot of total uncertainty in figure 10. The ANOVA results at the three selected points can be seen in table 6. Moreover, the pie charts in figure 12 show the contributions of the main and interaction effects of the factors in the total uncertainty. It is clear from table 6 that the blocking factor—stereoscopic camera angle—is the most significant factor ($F_0 = 301.65$, higher than $F_\mathrm{c} = 5.3$ with 95% confidence level) at the point I, as was also discussed by Prasad (2000) for stereoscopic PIV measurements. It is therefore important to select it optimally to minimize the related errors.

The factor Δt directly affects the out-of-plane displacement of the particles and it has relatively high contribution (23%) to the total uncertainty of the time-averaged velocity at the point II as shown in figure 12(b). However, its effect is not statistically significant for the stream-wise velocity component at 95% confidence level. It is to be noted that, high contribution of a factor to the total uncertainty does not guarantee the factor to be statistically significant at a certain confidence level. The statistical significance of a factor is estimated by comparing its mean square ($\mathrm{MS}_\mathrm{factor}$) with the error mean square MS_ε computing the F_0 value (shown in table 1) as: $F_0 = \mathrm{MS}_\mathrm{factor}/\mathrm{MS}_\varepsilon$. The F_0 value is then compared to the critical value F_c. Even for the same value of the $\mathrm{MS}_\mathrm{factor}$, the factor is statistically significant if $\mathrm{MS}_\mathrm{factor} \geqslant F_\mathrm{c}\ \mathrm{MS}_\varepsilon$, and statistically insignificant if $\mathrm{MS}_\mathrm{factor} < F_\mathrm{c}\ \mathrm{MS}_\varepsilon$. Therefore, the percentage contribution of a factor alone does not reveal its statistical significance. Nevertheless, the analysis for Y and Z velocity components shows that the factor Δt is significant in the regions of low flow fluctuations (the results are not shown for conciseness). In that case, the factor Δt influences the magnitude of the peak-locking error and, as observed by Legrand *et al* (2012), the regions of low flow fluctuations are those where the mean velocity is affected by peak-locking errors the most.

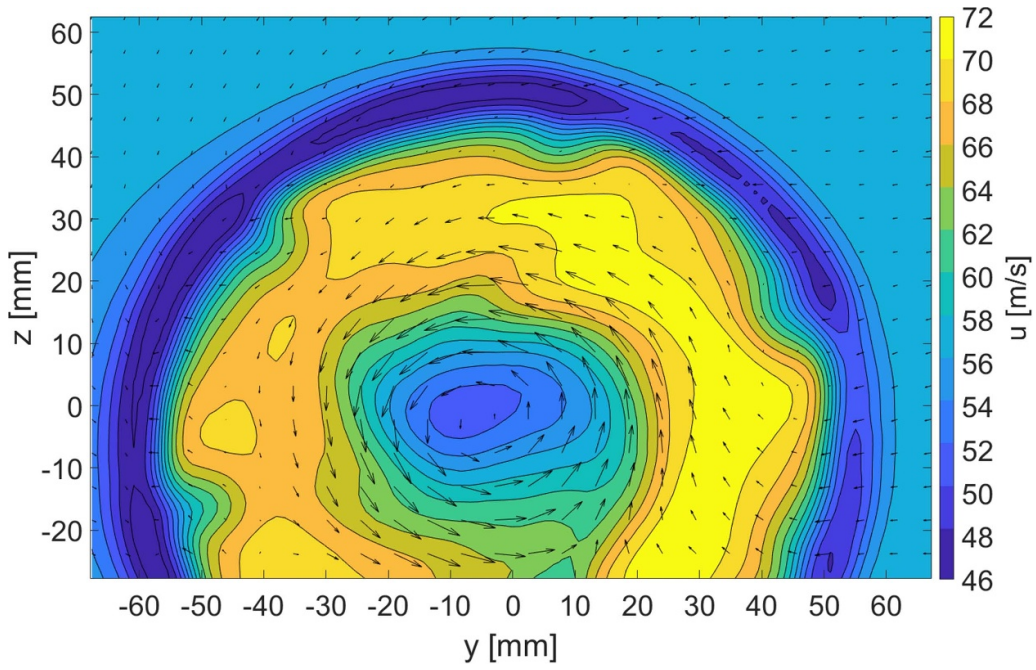

Figure 9. Time-averaged contour plots of the stream-wise velocity u and vector plots of the in-plane (Y–Z plane) velocity of the stereoscopic PIV measurements.

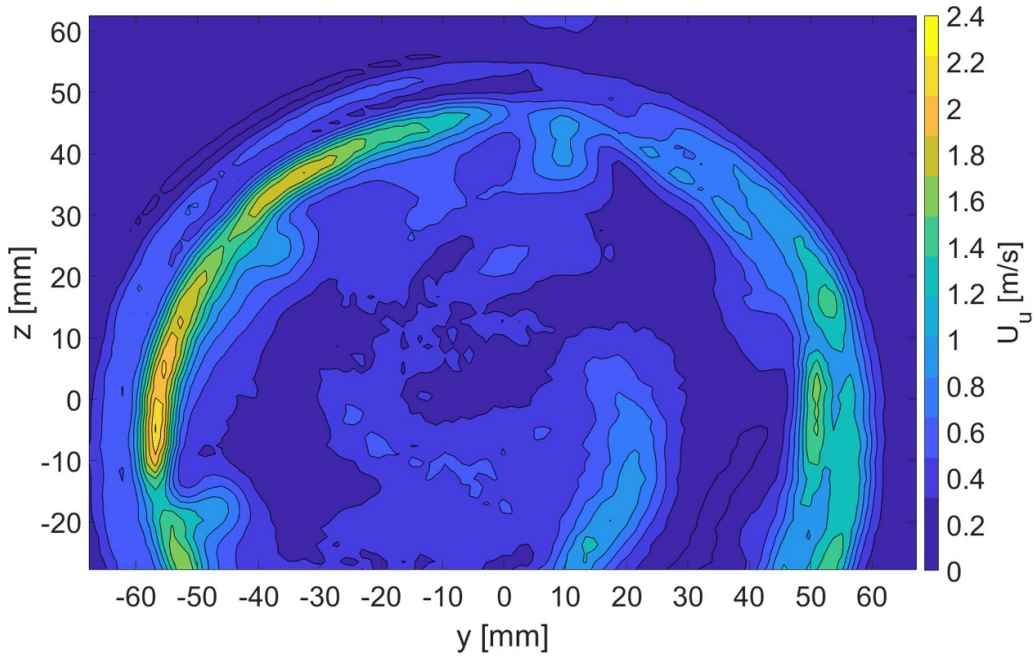

Figure 10. Total uncertainty in time-averaged stream-wise velocity u calculated by the proposed methodology.

The pie chart from figure 12(a) shows that, for the point I i.e. the flow region of low flow fluctuations, the blocking factor (i.e. the stereoscopic camera angle) contributes the most (97%) to the total uncertainty in the time-averaged stream-wise velocity. However, for the flow regions of high flow fluctuations i.e. the points II and III, the random error (due to the factors not directly considered in the analysis) has the biggest contribution of 57% and 71% to the total uncertainty in the mean stream-wise velocity, as shown in figures 12(b) and (c), respectively. This is due to the flow fluctuations in these regions being high which makes it difficult to segregate the contribution of individual systematic uncertainties. It is evident that in regions where the flow fluctuations are large, the random uncertainty of the mean velocity is also large due to the limited number of samples and therefore the limited statistical convergence. In these regions, the random errors dominate over the systematic error sources, as shown in figure 12 for points II and III. In contrast, in regions of low flow fluctuations

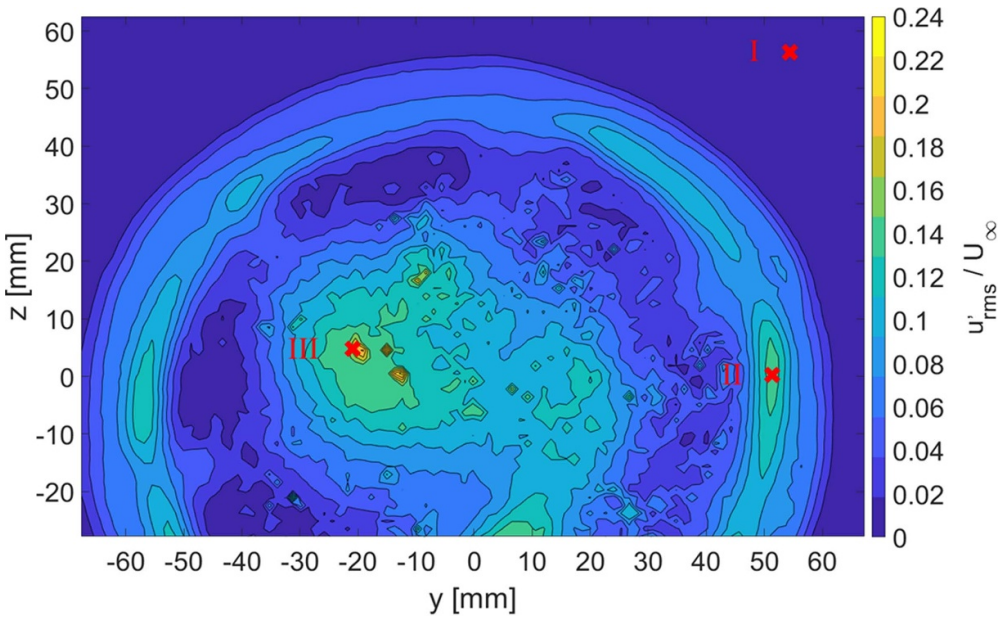

Figure 11. RMS of velocity fluctuations in stream-wise velocity normalized by freestream velocity.

Table 6. Analysis of Variances (ANOVA) results in the uncertainty quantification of time-averaged stream-wise velocity in the BLI propulsor experiment, where *A, B, C* and Block correspond to the factors: camera aperture *f*#, inter-frame time separation Δt, interrogation window size D_{I} and stereoscopic camera angle α, respectively (The critical value $F_{\mathrm{c}} = 5.3$ for 1 degree of freedom of numerator and 8 degrees of freedom of denominator at 95% confidence level (Montgomery 2013)).

		Point I				Point II				Point III			
Source	DoF	SS ($m^2\ s^{-2}$)	MS ($m^2\ s^{-2}$)	F_0	U_X ($m\ s^{-1}$)	SS ($m^2\ s^{-2}$)	MS ($m^2\ s^{-2}$)	F_0	U_X ($m\ s^{-1}$)	SS ($m^2\ s^{-2}$)	MS ($m^2\ s^{-2}$)	F_0	U_X ($m\ s^{-1}$)
A (*f*#)	1	0.00	0.00	0.60	0.02	1.25	1.25	0.46	0.29	0.17	0.17	0.48	0.11
B (Δt)	1	0.00	0.00	0.01	0.00	8.77	8.77	3.23	0.76	0.24	0.24	0.69	0.13
C (D_{I})	1	0.00	0.00	0.05	0.00	0.01	0.01	0.00	0.02	0.00	0.00	0.01	0.01
AB	1	0.01	0.01	1.40	0.02	0.55	0.55	0.20	0.19	0.02	0.02	0.07	0.04
AC	1	0.00	0.00	0.04	0.00	0.01	0.01	0.00	0.02	0.06	0.06	0.16	0.06
BC	1	0.00	0.00	0.21	0.01	0.10	0.10	0.04	0.08	0.25	0.25	0.72	0.13
Block	1	1.95	1.95	**301.65**	0.36	5.86	5.86	2.16	0.63	0.39	0.39	1.14	0.16
E	8	0.05	0.01	—	0.06	21.73	2.72	—	1.20	2.76	0.34	—	0.43
Total	15	2.01	0.13	—	0.37	38.27	2.55	—	1.60	3.89	0.26	—	0.51

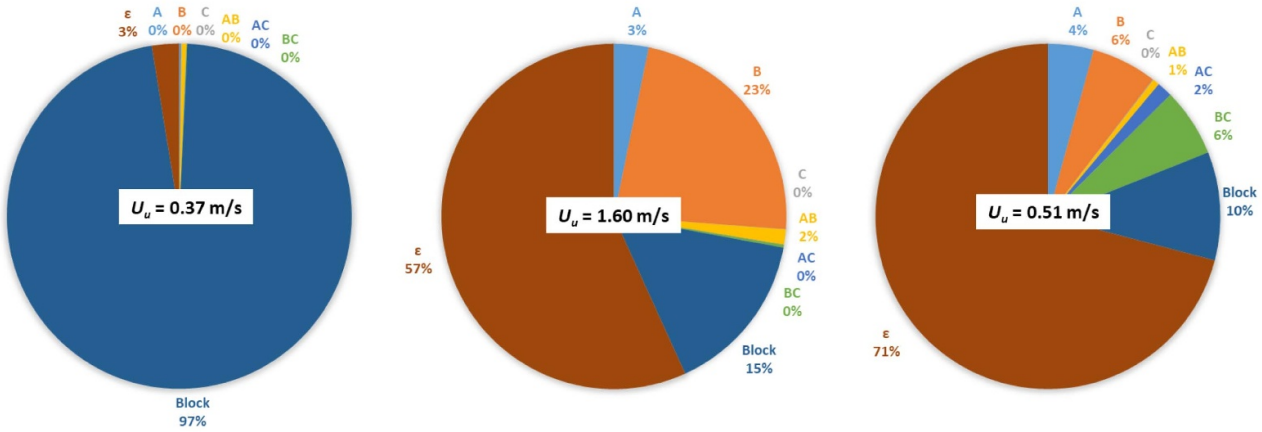

(a) Point I (potential flow region) (b) Point II (shear layer) (c) Point III (wake region)

Figure 12. Contribution of systematic uncertainties to the total uncertainty in time-averaged stream-wise velocity at the three points marked in figure 11, due to main and interaction effects of the factors-*A* (camera aperture *f*#), *B* (inter-frame time separation Δt), *C* (interrogation window size D_{I}) and block of stereoscopic camera angle α.

(e.g. point I of figure 12), the systematic error sources are expected to dominate.

5. Conclusions

A PIV UQ approach is proposed based on a statistical tool called DOEs. The basic principle of the approach is to measure a statistical quantity, ideally constant in time, for the different levels of experimental factors and to compute total variance and individual variances arising from the different levels of each of the factors. The proposed methodology is assessed for planar PIV measurements of the flow over a NACA0012 airfoil at 15 degrees angle of attack to quantify the uncertainty of the time-averaged velocity and Reynolds stress. Four design factors, namely camera aperture ($f\#$), inter-frame time separation (Δt), interrogation window size (D_I), laser sheet thickness (Δz), and a blocking factor of seeding density are considered for the analysis. It is found that the uncertainty of the mean velocity quantified by the DOE approach is significantly larger than random uncertainty estimated for one individual measurement from data statistics, which is ascribed to the capability of the DOE approach to account also for the systematic uncertainties. Additionally, the effect of the seeding density (block) has large contribution to the total uncertainty in the time-averaged stream-wise velocity everywhere in the flow domain. On the contrary, the factors Δt and Δz show significant contributions to the total uncertainty in the flow regions of low fluctuations and high fluctuations, respectively. In the case of Reynolds normal stress, it is found that the interrogation window size D_I and seeding density are the major contributors to the total uncertainty. The proposed methodology is also applied to the investigation by stereoscopic PIV of the flow at the outlet of a ducted BLI propulsor. The total uncertainties in time-averaged stream-wise velocities are computed along with the analysis of the effects of the experimental factors, namely camera aperture, inter-frame time separation, interrogation window size and stereoscopic camera angle. It is clear from the results that the stereoscopic camera angle has very significant contribution to the total uncertainty. Additionally, Δt is found to affect the total uncertainty in the flow regions of high fluctuations. The present work thus provides the ability to segregate the systematic uncertainties due to the experimental factors considered for the analysis. Knowing these constituent uncertainties, it will be possible to optimize the experiment in order to reduce the total uncertainty. The proposed methodology has been successfully used for planar (both 2 °C and 3 °C) PIV measurements. However, the approach is general and can be applied universally, irrespective of the kind of PIV setup for UQ in any of the measured quantities.

Data availability statement

The data that support the findings of this study are openly available at the following URL/DOI: 10.4121/20495787.v1 (Adatrao and Sciacchitano 2022) and 10.4121/20496108.v1 (Adatrao *et al* 2022).

Acknowledgments

The research is partly funded by the Dutch Research Organization NWO domain Applied and Engineering Sciences, Veni Grant 15854 Deploying Uncertainty Quantification in Particle Image Velocimetry.

ORCID iDs

Sagar Adatrao https://orcid.org/0000-0002-8593-3920
Andrea Sciacchitano https://orcid.org/0000-0003-4627-3787

References

Adatrao S and Sciacchitano A 2022 MATLAB scripts created during the work on "Design of experiments: a statistical tool for PIV uncertainty quantification" *4TU.ResearchData* Software (https://doi.org/10.4121/20495787.v1)

Adatrao S, Sciacchitano A and Bertone M 2021 Multi-Δt approach for peak-locking error correction and uncertainty quantification in PIV *Meas. Sci. Technol.* **32** 054003

Adatrao S, van der Velden S, van der Meulen M J, Cruellas Bordes M and Sciacchitano A 2022 Figures created during the work on "Design of experiments: a statistical tool for PIV uncertainty quantification" *4TU.ResearchData* Dataset (https://doi.org/10.4121/20496108.v1)

Aeschliman D and Oberkampf W 1998 Experimental methodology for computational fluid dynamics code validation *AIAA J.* **36** 733–41

Beresh S J 2009 Comparison of PIV data using multiple configurations and processing techniques *Exp. Fluids* **47** 883–96

Bhattacharya S, Charonko J J and Vlachos P P 2016 Stereoscopic-particle image velocimetry uncertainty quantification *Meas. Sci. Technol.* **28** 015301

Bhattacharya S, Charonko J J and Vlachos P P 2018 Particle image velocimetry (PIV) uncertainty quantification using moment of correlation (MC) plane *Meas. Sci. Technol.* **29** 115301

Charonko J J and Vlachos P P 2013 Estimation of uncertainty bounds for individual particle image velocimetry measurements from cross-correlation peak ratio *Meas. Sci. Technol.* **24** 065301

Coleman D E and Montgomery D C 1993 A systematic approach to planning for a designed industrial experiment *36th Annual Fall Technical Conf.* (*Philadelphia, PA, USA*, *8–9 October*)

DeBonis J R, Oberkampf W L, Wolf R T, Orkwis P D, Turner M G B H and Benek J A 2012 Assessment of computational fluid dynamics and experimental data for shock boundary-layer interactions *AIAA J.* **50** 891–903

DeLoach R 2000 The modern design of experiments: a technical and marketing framework *21st AIAA Advanced Measurement Technology and Ground Testing Conf.* (*Denver, CO, USA*, *19–22 June*)

DeLoach R and Micol J R 2011 Comparison of resource requirements for a wind tunnel test designed with conventional vs. modern design of experiments method *49th AIAA Aerospace Sciences Meeting* (*Orlando, FL, USA*, *4–7 January*)

DeLoach R, Obara C J and Goodman W 2012 A practical methodology for quantifying the random and systematic components of unexplained variance in a wind tunnel *50th AIAA Aerospace Sciences Meeting and Exhibit* (*Nashville, TN, USA*, *9–12 January*)

Kähler C J, Astarita T, Vlachos P P, Sakakibara J, Hain R, Discetti S, Foy R and Cierpka C 2016 Main results of the 4th international PIV challenge *Exp. Fluids* **57** 1–71

Legrand M, Nogueira J, Ventas R and Lecuona A 2012 Simultaneous assessment of peak-locking and CCD readout errors through multiple Δt strategy *Exp. Fluids* **53** 121–35
Montgomery D C 2013 *Design and Analysis of Experiments* 8th edn (New York: Wiley)
Neal D R, Sciacchitano A, Smith B L and Scarano F 2015 Collaborative framework for PIV uncertainty quantification: the experimental database *Meas. Sci. Technol.* **26** 074003
Nogueira J, Lecuona A, Nauri S, Legrand M and Rodriguez P A 2011 Quantitative evaluation of PIV peak locking through a multiple Δt strategy: relevance to the rms component *Exp. Fluids* **51** 785–93
Oberkampf W L and Roy C J 2010 *Verification and Validation in Scientific Computing* (Cambridge: Cambridge University Press)
Prasad A K 2000 Stereoscopic particle image velocimetry *Exp. Fluids* **29** 103–16
Rhode M N and Oberkampf W L 2012 Estimation of uncertainties for a supersonic retro- propulsion model validation experiment in a wind tunnel *42nd AIAA Fluid Dynamics Conf. and Exhibit* (*New Orleans, LA, USA*, *5–28 June*)
Scarano F 2002 Iterative image deformation methods in PIV *Meas. Sci. Technol.* **13** R1–R19
Scharnowski S, Sciacchitano A and Kähler C J 2019 On the universality of Keane & Adrian's valid detection probability in PIV *Meas. Sci. Technol.* **30** 035203
Sciacchitano A 2019 Uncertainty quantification in particle image velocimetry *Meas. Sci. Technol.* **30** 092001
Sciacchitano A, Neal D R, Smith B L, Warner S O, Vlachos P P, Wieneke B and Scarano F 2015 Collaborative framework for PIV uncertainty quantification: comparative assessment of methods *Meas. Sci. Technol.* **26** 074004
Sciacchitano A and Wieneke B 2016 PIV uncertainty propagation *Meas. Sci. Technol.* **27** 084006
Sciacchitano A, Wieneke B and Scarano F 2013 PIV uncertainty quantification by image matching *Meas. Sci. Technol.* **24** 04530
Smith B L and Oberkampf W L 2014 Limitations of and alternatives to traditional uncertainty quantification for measurements *The ASME 2014 Fluids Engineering Summer Meeting* (*Chicago, IL, USA*, *3–7 August*)
Timmins B H, Wilson B W, Smith B L and Vlachos P P 2012 A method for automatic estimation of instantaneous local uncertainty in particle image velocimetry measurements *Exp. Fluids* **53** 1133–47
Tummers M J 1999 Investigation of a turbulent wake in an adverse pressure gradient using laser Doppler anemometry *PhD Thesis* Delft University Press
Wieneke B 2005 Stereoscopic-PIV using self-calibration on particle images *Exp. Fluids* **39** 267–80
Wieneke B 2015 PIV uncertainty quantification from correlation statistics *Meas. Sci. Technol.* **26** 074002